Interactions of E. coli with cylindrical micro-pillars of different geometric modifications

Venkata Rao Krishnamurthi[a], Nathaniel Harris[b], Ariel Rogers[a], Min Zou[b,c], Yong Wang[a,c,d,*]

[a]Department of Physics, [b]Department of Mechanical Engineering, [c]Materials Science and Engineering Program, [d]Cell and Molecular Biology Program, University of Arkansas, Fayetteville, AR 72701.

[*]Corresponding author. Email: yongwang@uark.edu

Abstract

Understanding the behavior of bacteria at the proximity of different surfaces is of great importance and interest. Despite recent exciting progress in geometric control of bacterial behavior around surfaces, a detailed comparison on the interaction of bacteria with cylindrical surfaces of different geometric modifications is still missing. Here, we investigated how bacteria interacted with cylindrical micro-pillars and modified cylindrical micro-pillars with sprocket, gear, and flower-like wall surface features. Using phase-contrast microscopy, we examined the motion of bacteria around the micro-pillars, and observed different responses of bacteria to each geometric modification. In addition, we extracted the trajectories of the bacteria and characterized several parameters (instantaneous velocity v, change of direction δ, approaching angle ϕ) to quantitatively compare the effects of the geometric modifications on the micro-pillars. We found that sharp spikes showed the largest effect, compared to smooth surface, convex and concave ripples. Lastly, we carried out numerical simulations, which explained the experimental observations and showed that the observed effects were due to the geometric modifications.

Keywords: microstructures, 3D printing, surface, geometry, two-photon polymerization

Word count: 5791. Number of figures: 7. Number of tables: 0.

Introduction

Motility is critical to many bacteria for pursuing nutrients and avoiding hazards. To move in aqueous environment with various obstacles and surfaces, some bacteria, such as *Escherichia coli* (*E. coli*), rely on flagella, which consist of motors and filaments, extending out several cell body lengths into the environment [1–3]. In the past few decades, extensive efforts have been made to understand the bacterial motility from many aspects, including bacterial behavior and molecular machineries and mechanisms in liquid media, bacterial swarming on solid or semi-solid surfaces, changes of bacterial behaviors and their mechanisms at the interfaces between liquid media and solid surfaces, navigation of bacteria in porous structures, and formation of biofilms and bacterial streamers at surfaces or around objects [1,4–15].

It is important to understand the behavior of bacteria at the proximity of surfaces or objects for several reasons. First, bacteria swim differently when they are close to surfaces compared to in the bulk [7,8,16–19]. For example, curved trajectories were observed for *E. coli* bacteria when they were near planar surfaces [7]. Second, understanding the interaction of bacteria with

surfaces and objects provides useful insight into controlling bacteria [20–24]. A recent study demonstrated the use of teardrop posts/pillars to guide the motion of microscale swimmers [25]. Third, a better understanding of the bacterial interaction with surfaces and objects will benefit biomedical applications, such as preventing the formation of biofilm, biofouling, and streamers, or creating surfaces that are coated with bactericidal reagents and capable of trapping bacteria for longer treatment duration [9,26–29], which may open new avenues for better fighting against antibiotic resistant microbes.

In recent years, exciting progress has been made in controlling bacterial behavior by simple geometries [20–23,25,30]. Micro-fabricated walls with funnel-shaped openings were designed to produce net directional flux of swimming bacteria, leading to a buildup of the concentration of the bacteria [21]. In addition, it was found that circular/convex walls were able to trap swimming bacteria in a curvature-dependent manner [31]; however, it was unclear how modifications on the convex walls would affect the trapping. Furthermore, it was reported that cylindrical micro-pillars facilitate the formation of bacterial streamers in long terms (typically >100 s), which are flow-mediated slender structures of bacteria encased in self-secreted matrix of extracellular polymeric substances (EPS) [12,32,33]; however, the short-term dynamics of bacteria and their interactions with the micro-pillars were rarely quantified. More recently, it was demonstrated that locally varying boundary curvature changed the accumulation dynamics of swimming bacteria on surfaces [20]; on the other hand, the examined variations were on planar/flat boundaries. By changing the cylindrical posts into teardrop pillars, it was possible to guide the motion of microswimmers [25], indicating the importance of surface modifications on the cylindrical walls, although a detailed comparison on the interaction of bacteria with cylindrical surfaces of different geometric modifications is still missing.

To promote a better understanding of the interactions of bacteria with cylindrical surfaces with different geometric features, we quantitatively investigated how bacteria interact with cylindrical micro-pillars with different wall modifications (Figure 1). The micro-pillars were approximately 20 μm in diameter with a height of 60 μm, arranged in arrays with a center-to-center distance of 40 μm. Four different wall features (Figure 1B) were examined in this study, including smooth circles (CIRC; no modification), convex ripples (CVEX), concave ripples (CCAV), and sharp spikes (SSPK). We monitored the motion of *E. coli* bacteria around these micro-pillars using phase-contrast microscopy, and observed different responses of bacteria to different surface modifications. In addition, we extracted the trajectories of the bacteria and compared the bacterial interactions using quantitative parameters, including the instantaneous velocity of the bacteria (v), the change of direction (δ) of the bacteria, and the approaching angle of the bacteria to the micro-pillars (ϕ). We found that sharp spikes resulted in the largest changes in the bacterial behavior at the vicinity of the micro-pillars. Lastly, to understand the experimental observations, we performed numerical simulations and showed that the observed differences in interactions could be attributed to geometric modifications on the circular micro-pillars.

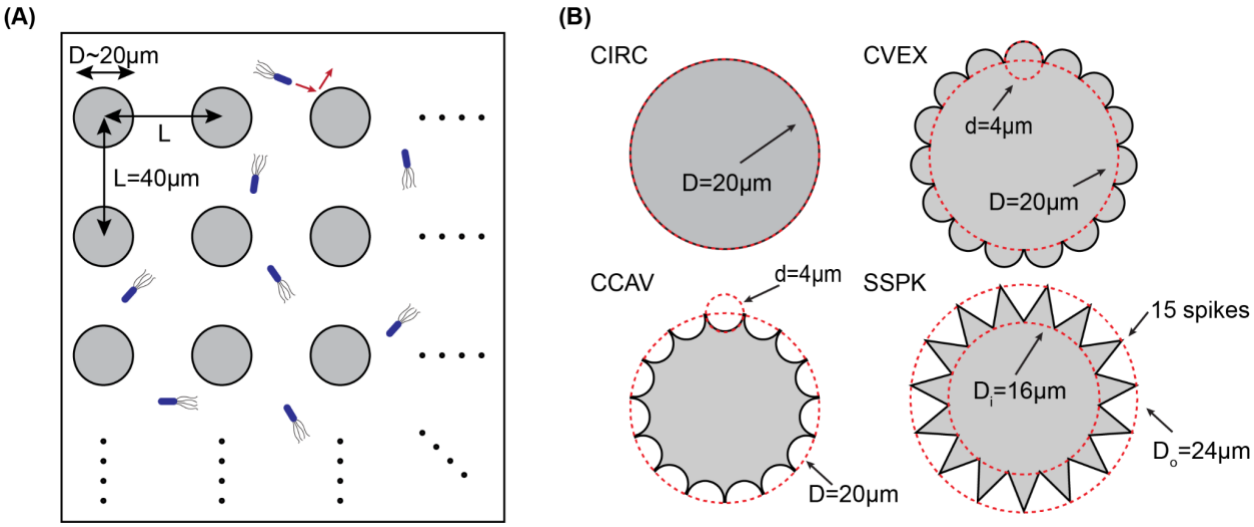

Figure 1. Sketch of this study and design of micro-pillars. (**A**) Sketch for studying the interaction of bacteria with arrays of micro-pillars with diameters of ~20 μm and center-to-center distance of ~40 μm. (**B**) Designs of micro-pillars with four types of wall features: smooth circles (CIRC), convex ripples (CVEX), concave ripples (CCAV), and sharp spikes (SSPK).

Materials and Methods

Bacterial strain and growth

An *E. coli* K12-derived strain (YW0092) [34–36] was used in this study. Each experiment started with inoculating a single bacterial colony into 5 mL of Luria Broth (LB) medium (MilliporeSigma, USA) supplemented with kanamycin and chloramphenicol (50 μg/mL and 34 μg/mL, respectively). The liquid culture was grown at 37°C in a shaking incubator (250 RPM) overnight. On the second day, the overnight culture was diluted by 5000 into 5mL of fresh LB medium with antibiotics. The new culture was grown at 32°C in the shaking incubator until the bacterial culture reached OD_{600} ≈ 0.2 for imaging.

Design and fabrication of micro-pillar master

Micro-pillars with different wall features were designed in SolidWorks (Dassault Systèmes, France). Briefly, circular micro-pillars with a diameter of 20 μm, a height of 60 μm, and a center-to-center distance of 40 μm were first designed as the control for comparison (Figure 1B, CIRC). Then, circular extrusions along the perimeter resulted in micro-pillars with convex-ripples (flower-like), while circular cuts resulted in micro-pillars with concave-ripples (sprocket-like) (Figure 1B, CVEX and CCAV). Triangular extrusions resulted in micro-pillars with sharp-spikes (pointed gear-like) (Figure 1B, SSPK). The footprint area of each micro-pillar array was 2x2 mm, and the edge of each array was separated by 1 mm from neighboring arrays to limit inter-array interaction.

The designs of the micro-pillars were fabricated with a 3D nanoprinter (PhotonicProfessional GT System, Nanoscribe GmbH, Germany) to serve as the master surfaces for replicate molding. The nanoprinter uses a near infrared (NIR) femtosecond laser (780 nm, 100 fs, 150 mW) to harden UV-sensitive polymers through a two-photon polymerization (2PP) process. As illustrated in Figure 2A, a 25x immersion lens was used to converge the NIR laser into an ellipsoidal voxel with an average width of 600 nm and average height of 2 μm [37]. IP-Dip (Nanoscribe GmbH,

Germany), an optimized photoresist for 2PP printing from Nanoscribe, was chosen as the master printing material. According to the accompanying Material Safety Data Sheet (MSDS), it contains 2-(hydroxymethyl)-2-[[(1-oxoallyl)oxy]methyl]-1,3-propanediyl diacrylate, 9H-fluorene-9,9-diylbis(4,1-phenyleneoxyethane-2,1-diyl)-bisacrylate, and biphenyl-2-ol, ethoxylated, esters with acrylic acid. Indium tin oxide (ITO) coated glass (25x25 mm) was cleaned using acetone and then isopropyl alcohol, and rinsed three times using deionized water, followed by oxygen plasma cleaning for 1 minute. The printed micro-pillar master was soaked in propylene glycol methyl ether acetate for 10 minutes followed by soaking in isopropyl alcohol for 2 minutes. The printed micro-pillar master was then post-exposed under 300 mW/cm^2 UV light for 2 minutes to fully crosslink the micro-pillars [38].

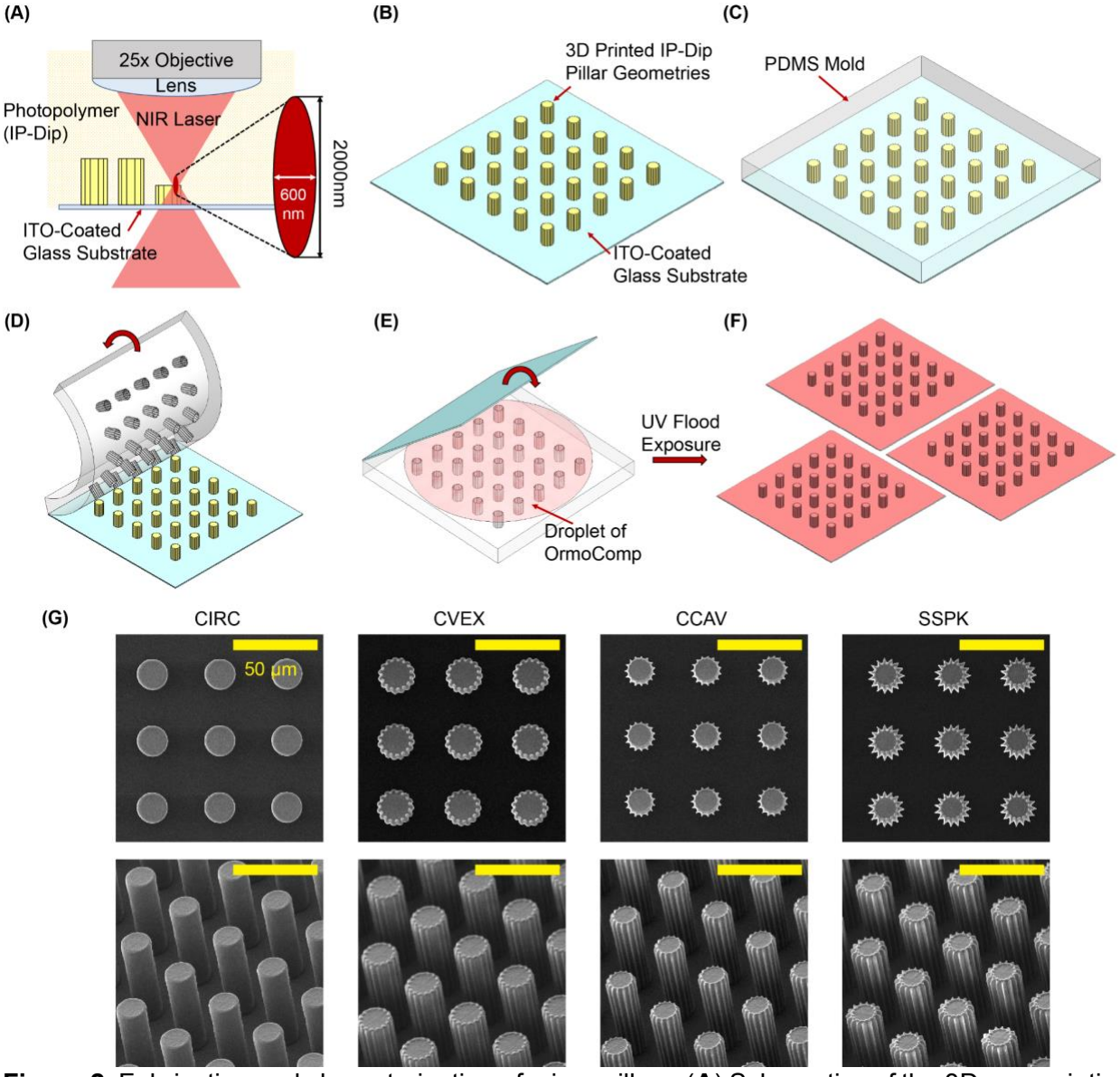

Figure 2. Fabrication and characterization of micro-pillars. (**A**) Schematics of the 3D nanoprinting process by 2PP showing the resolution size of the printing voxel. (**B**) A conceptual view of the 3D printed IP-Dip micro-pillar master showing one design as an example. (**C**) PDMS mold cast and set onto the IP-Dip master. (**D**) Removal of the PDMS mold. (**E**) The process used to mold

replicate samples of micro-pillar arrays that includes placement of a droplet of OrmoComp onto the mold, evacuation of the entrapped air out of the mold, placement of an OrmoPrime-glass slide on top of the OrmoComp, and UV flood exposure in order to crosslink the OrmoComp. (**F**) Replicated micro-pillars. (**G**) SEM images of the micro-pillars with different surface features. Top: top view; bottom: isometric view. Scale bars = 50 μm.

PDMS molding of micro-pillars

To quickly fabricate multiple samples, a PDMS mold was made from the 3D printed micro-pillar master. OrmoComp (Micro Resist Technology GmbH, Germany), a biocompatible and optically transparent UV-sensitive polymer, was chosen as the replication material. According to its MSDS, OrmoComp contains anisole, 2,2-bis(acryloyloxymethyl)butyl acrylate, trimethylolpropane triacrylate, and diphenyl(2,4,6-trimethylbenzoyl)phosphine oxide. The replication process is shown in Figure 2B–2F. First, 22x22 mm No. 1.5 glass cover slips (VWR International) were cleaned using the same progressive rinse and surface activation procedure described previously, and a thin layer of OrmoPrime (Micro Resist Technology GmbH, Germany), an adhesive tailored for use with OrmoComp photoresist, was spin-coated onto the clean glass surfaces at 4000 rpm for 1 minute. The samples were immediately placed onto a hotplate and hard baked at 150°C for 5 minutes, then set aside to cool in ambient air. A droplet of OrmoComp was then placed onto the PDMS mold and trapped air was vacuumed out of the pillar-shaped cavities with a vacuum pressure of -635 mmHg for 2 hours. Every half an hour, large air bubbles that did not break the surface were removed using forceps. After air was evacuated from the mold, an OrmoPrime-treated glass surface was then placed on top of the OrmoComp and set aside for 10 minutes to ensure even distribution of photoresist underneath the cover glass. Samples were then cured under 300 mW/cm^2 light intensity for 5 minutes, removed from the mold and post-cured for an additional 5 minutes to ensure complete crosslinking of the photoresist. The micro-pillar samples were then characterized by optical microscopy (VK-X260K, Keyence Corporation, Japan) and scanning electron microscopy (VEGA3, TESCAN Corporation, Czech Republic).

Phase contrast microscopy

The coverslip with the OrmoComp micro-pillars was glued to a petri-dish (Cell E&G LLC, USA) with a circular hole with a diameter of 13 mm (Figure 3A), and then coated with bovine serum albumin (BSA, Sigma-Aldrich, USA) by incubating 1 mg/mL BSA solution in phosphate-buffered saline (PBS, Sigma-Aldrich, USA) for 5 min. After discarding the BSA solution and washing the petri-dish with PBS, 2 mL *E. coli* bacteria ($OD_{600} \approx 0.2$) in LB medium were added to the petri-dish, and imaged using a phase contrast microscope (Olympus IX-73 inverted microscope, Olympus Corporation, Japan) equipped with a 100x, NA=1.25 phase-contrast, oil-immersion objective (Olympus Corporation, Japan) and an EMCCD camera (Andor Technology, UK). The objective was focused at the bottom of the micro-pillars (Figure 3B), ~2.2 μm from the top surface of the coverslip. The microscope and data acquisition were controlled using Micro-Manager [39,40]. The exposure time was set to 15 ms, resulting in an actual time difference of 39.6 ms between adjacent frames, while the number of frames of each acquired movie was 5000.

When monitoring the motion of bacteria using phase-contrast microscopy, we chose to focus around the bottom of the micro-pillars (~2.2 μm from the top surface of the coverslip) for two reasons. First, it was shown that the actual concentration of bacteria at the vicinity of the flat surface is higher than the bulk [16–19], providing a higher number of bacteria for analysis. Second, compared to bacteria swimming in the bulk of the medium, bacteria moving around the

flat surface showed much lower frequency of getting out of the focal plane [16–19], generating longer trajectories. Both reasons give better statistics for quantitative comparisons.

Image processing and tracking of bacteria

The acquired movies were first processed using ImageJ [41,42]. First, the movies were rescaled to half (i.e., from 512x512 to 256x256), resulting in an effective pixel size of 0.32 μm. This step was performed to reduce the requirement of computation memory and time for later steps. Next, the average images of every 1000 frames in the movies were computed in ImageJ [41,42], which highlighted the micro-pillars and were used to identify the location of the micro-pillars. Then, the average images (i.e., micro-pillars) were subtracted from the original images of the rescaled movies, resulting in images (and movies) showing only the moving bacteria. The last two steps significantly facilitated the automated detection and tracking of bacteria.

The bacteria were detected using custom Python scripts [43] based on the *scikit-image* Python package [44]. Briefly, for each frame of the processed movies, the background was first removed using a rolling-ball algorithm [45] with a ball size of 3 pixels, followed by smoothing twice using a Gaussian filter with a standard deviation of 1 pixel. The background in the smoothed image was removed once again, followed by applying a threshold to obtain a black/white (BW) image. Edges were detected from the BW image using the Sobel filter [46], followed by dilating the edges by 1 pixel to fill possible gaps in the edges. Small objects with areas <50 pixels were removed, before performing a flood fill [47]. The filled objects were eroded with 3 pixels, followed by removing small objects (area <50 pixels). The resulting BW image was segmented into individual ones, which corresponded to the identified bacteria. The locations (x, y) of the bacteria, as well as their corresponding frames, were recorded and then linked into trajectories with *trackpy* [48], using a maximum displacement between adjacent frames of 5 pixels (1.6 μm) and a memory of 3 frames. The trajectories of the bacteria were saved and used for computations of the instantaneous velocities, changes of moving direction, and approaching angles of the bacteria.

Simulation of bacteria interacting with circular micro-pillars with or without surface modifications

The simulation of bacteria in the presence of micro-pillars were carried out using custom MATLAB programs based on Volpe et al. [49]. Briefly, a micro-pillar (~20 μm in diameter, Figure 1B) was placed at the center of a region of 80x80 μm^2, with 30 spherical bacteria (radius R = 1 μm) randomly placed outside the micro-pillar. The size of the simulation region (L = 80 μm) was similar to the size of the field of view in our experiments (81.92 μm). Each bacterium was modeled as a sphere whose kinematics were described by the bacterial orientation θ and its location (x, y). For simplicity and convenience, periodic boundary conditions were applied when a bacterium moved out of the region (i.e., $x \to x - L$ if $x > L/2$, or $x \to x + L$ if $x < -L/2$; similar for y).

In the simulations, the orientation and position of a bacterium at time step i was determined by its previous step $i-1$ following Volpe et al. [49]. First, we calculated tentative orientation (θ_i) and location (x_i, y_i) of the bacteria at step i: $\theta_i = \theta_{i-1} + \Omega\,\Delta t + \sqrt{2D_R\,\Delta t}\;\xi_{\theta i}$, $x_i = x_{i-1} + v\cos\theta_{i-1}\,\Delta t + \sqrt{2D_T\,\Delta t}\;\xi_{xi}$ and $y_i = y_{i-1} + v\sin\theta_{i-1}\,\Delta t + \sqrt{2D_T\,\Delta t}\;\xi_{yi}$, where $\Delta t = 0.02$s is the time step size, Ω is the rotational angular velocity, $D_R = \frac{k_B T}{8\pi\eta R^3}$ is the rotational diffusion coefficient, $v = 15$ μm/s is the translational speed, $D_T = \frac{k_B T}{6\pi\eta R}$ is the translational diffusion coefficient, $\eta = 10^{-3}$Pa·s is the viscosity of the medium, k_B is the Boltzmann constant, $T = 300$K

is the temperature, ξ's are random numbers from a Gaussian distribution with a mean of 0 and a standard deviation of 1 [49]. If the bacterium did not collide with the micro-pillar, the tentative values were taken; however, if the bacterium collided with the micro-pillar, the tentative bacterial location (x_i, y_i) was reflected at the boundary of the micro-pillar to the location at step i as described in [49]. The boundaries of micro-pillars were obtained from the bitmap image of the micro-pillar design (Figure 1B).

For each simulation, 10000 steps with a step size of 20 ms were performed, and the locations of the bacteria were recorded, followed by trajectory identification and quantitative analysis the same way as the experimental data. In different simulations, we varied the type of micro-pillars or the rotational angular velocity Ω of bacteria.

Results and Discussion

Images of micro-pillars

The fabricated micro-pillars were imaged and examined by scanning electron microscopy (SEM, Figure 2G) and optical microscopy (Figure S1). The images show that the micro-pillars were satisfactorily printed as designed. The printer's x-y resolution is 600 nm, so the points of the CCAV and SSPK designs show some variations due to the very small cross-sectional area at the pointed tips. Examination of the isometric views of each pillar design reveals that the wall geometries were printed and molded consistently, even with an aspect ratio of 3:1 and fine wall features. The repeatability of the molded pillar geometries is key to ensure the bacteria interact with a consistent pillar design, and to correctly understand the effects of the different wall geometries on bacterial motility.

Bacterial trajectories

Examples of bacterial trajectories were shown in Figure 3C–3I. Each colored line represents a single trajectory of a bacterium (Figure 3C). Note that a bacterium may contribute to multiple trajectories due to its disappearance and reappearance (e.g., moving out of and later into the focal plane). The results for bacteria moving on a flat surface without any micro-pillars were shown as the control (Figure 3D). We observed that the trajectories of the bacteria far away from the micro-pillars were similar to those in the control, displaying directional but curved motion with occasional random changes of directions. This observation was consistent with previous reports, and could be attributed to the combination of Brownian dynamics and run-and-tumble dynamics [7,16]. In contrast, significant differences were observed for the trajectories of bacteria at the vicinity of the micro-pillars. For example, the bacterial trajectories around the CIRC and CVEX micro-pillars were shown as smooth curves along the tangent of the micro-pillars (Figure 3E, 3F, and 3I), while bacteria around the CCAV and SSPK showed aggregation of trajectories (Figure 3G, 3H, and 3I). The aggregation of the trajectories (highlighted by red arrows in Figure 3I) indicates that the bacteria were trapped around the CCAV and SSPK micro-pillars. The differences in the bacteria trajectories around different micro-pillars implied that the bacteria interact differently with the different surface modifications.

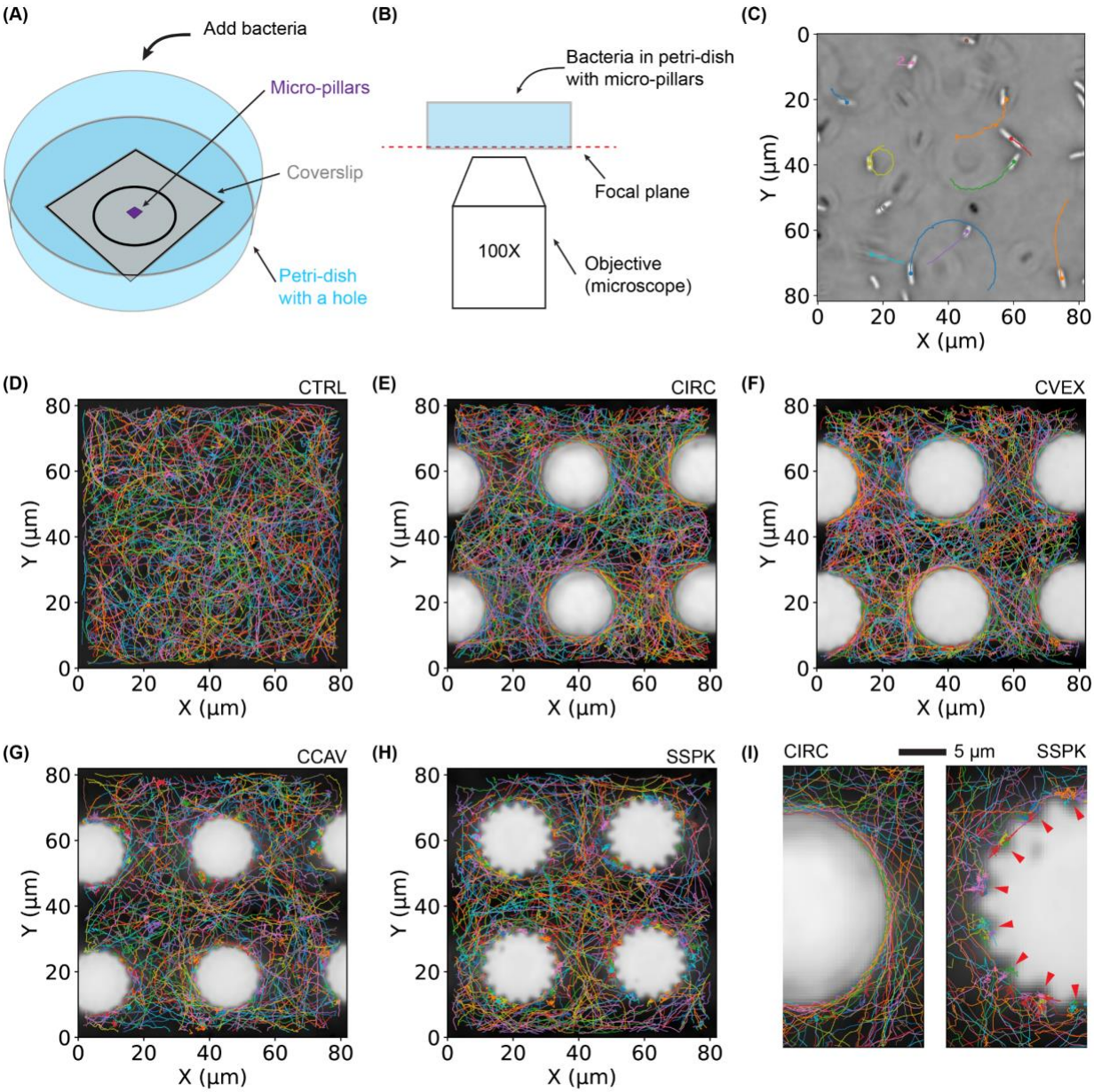

Figure 3. Sketch of imaging setup and examples of bacterial trajectories. (**A**) A coverslip (gray) with the micro-pillars (purple) was glued to a petri-dish (blue) with a hole, followed by adding bacteria in LB medium for phase-contrast imaging. (**B**) Objective of the microscope was focused at the bottom of the micro-pillars (i.e., the top surface of the coverslip of the petri-dish). (**C**) Examples of individual trajectories (with different colors) with the corresponding bacteria (bright rod-shapes) indicated by colored dots. (**D–H**) Random examples of individual bacterial trajectories in the (**D**) absence and (**E–H**) presence of micro-pillars with different surface features. Different colors indicate different trajectories. (**I**) Comparison of bacterial trajectories at the vicinity of a CIRC micro-pillar and an SSPK micro-pillar, showing aggregation of trajectories around the SSPK micro-pillar as highlighted by red arrows.

Instantaneous velocity of bacteria

To quantify the differences observed in the experiments, we estimated and compared the instantaneous velocity (v) of bacteria, $v(t) = \frac{|\vec{r}(t+\Delta t)-\vec{r}(t)|}{\Delta t}$, where $\vec{r}(t)$ is the position of the bacteria at time t, and Δt is the time interval between adjacent frames. The hypothesis is that the instantaneous velocities of bacteria would be lower for the trapped bacteria by the micro-pillars. To test this hypothesis, we first compared the distributions of the velocities. As the behavior of the bacteria far away from the micro-pillars were similar to the control for all the different types of micro-pillars, we split the instantaneous velocities into two groups based on a cutoff ε measured from the micro-pillar (inset of Figure 4A). For each instantaneous velocity, we calculated the distance from the corresponding position of the bacterium to the surface of the micro-pillars, Δr. If $\Delta r \leq \varepsilon$, this velocity was classified into the group of v_{in} (i.e., inside of the cutoff circle); otherwise (i.e., outside of the cutoff circle), the velocity was grouped as v_{out}. The distributions of v_{in} and v_{out} with a cutoff of ε = 4.8 μm (15 pixels) are shown in Figure 4A and 4B, respectively. We observed that, compared to the control, the peaks of the v_{in}-distributions clearly shifted to the left for the CCAV and SSPK micro-pillars, confirming that the interaction of bacteria with these micro-pillars reduced the velocities of the bacteria. The CVEX micro-pillars resulted in a small left shift in the v_{in}-distribution, but not as significant as the CCAV and SSPK micro-pillars. Also, the v_{in}-distribution for the CIRC micro-pillars was similar to the control. In contrast, outside the cutoff, the distributions of the velocities (v_{out}) were not different for all the micro-pillars, compared to the control (Figure 4B).

In addition to the overall distribution of the instantaneous velocities, we examined the dependence of average bacterial velocity on the distance of the bacteria to the surface of the micro-pillars (Δr). As shown in Figure 4C, the average velocity (v_{in}) decreased quickly as Δr decreased (i.e., as the bacteria were closer to the surface) for the SSPK and CCAV micro-pillars, while it remained roughly flat for the CIRC micro-pillars. The v_{in} vs. Δr curve for the CVEX micro-pillars was in the middle. Consistent with the results from overall distributions, we observed little difference for v_{out} vs. Δr curves for the different surface modifications on the micro-pillars (Figure 4D). These results supported our hypothesis that the trapping interactions of certain geometric modifications on the micro-pillars slowed down the motion of the bacteria. It is worth pointing out that these results were robust: varying the cutoff from 3.2 μm (10 pixels) to 6.4 μm (20 pixels) did not change the results significantly (Figure S2).

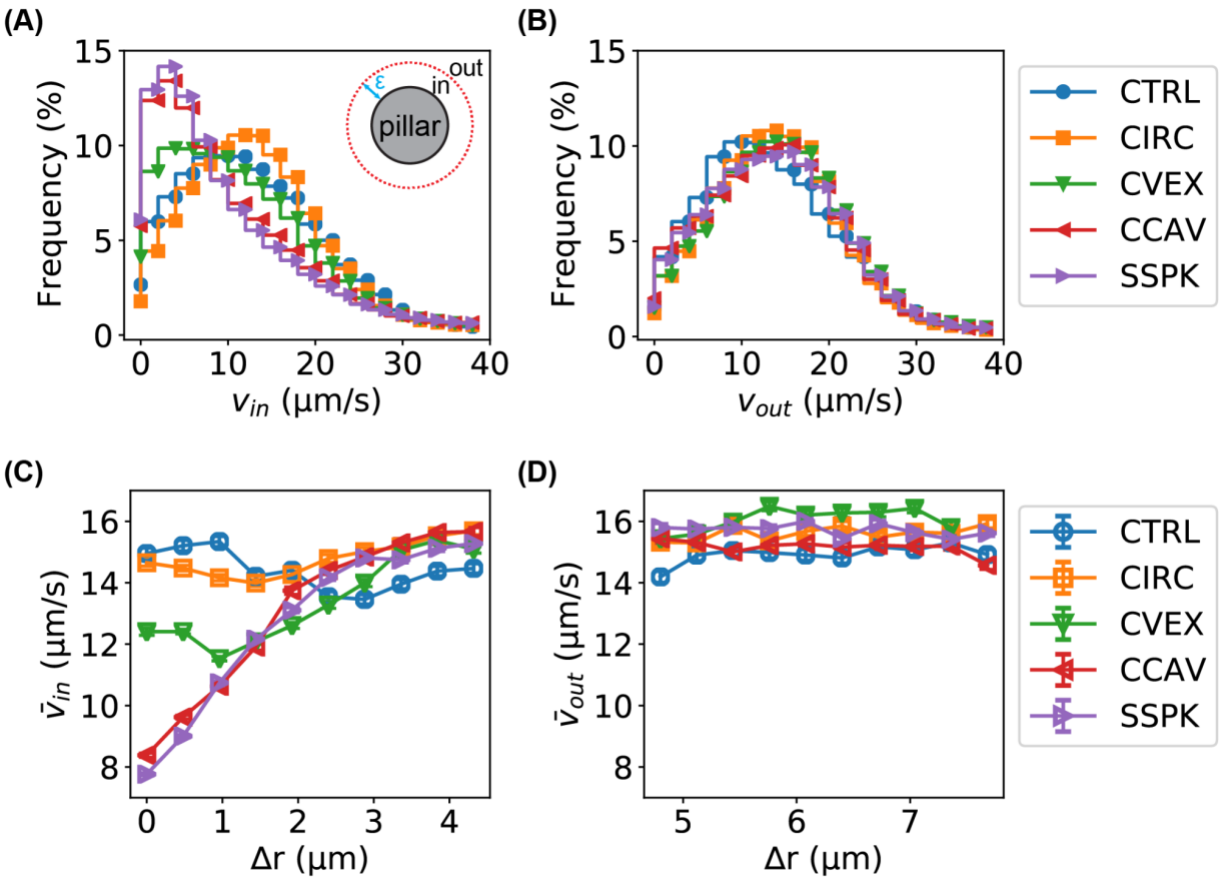

Figure 4. Comparison of instantaneous velocities (v) of bacteria when interacting with micro-pillars with different surface modifications. (**A, B**) Distribution of bacterial velocities inside (v_{in}) or outside (v_{out}) of a virtual cutoff boundary (ε = 4.8 μm). Inset: illustration of inside and outside of the cutoff boundary. (**C, D**) Dependence of the mean bacterial velocities on the distance of the bacteria to the surface of the micro-pillars. Error bars (smaller than the symbols) represent the standard errors of the means.

Change of moving direction of bacteria

We also hypothesized that the run-and-tumble dynamics of the bacteria were affected by their interactions with the different surface features of the micro-pillars. To test this hypothesis, we estimated the change of moving direction of the bacteria (per frame) [50–52], $\delta = cos^{-1}\left(\frac{\vec{v}_{i+1}\cdot\vec{v}_i}{v_{i+1}\,v_i}\right)$. Because the bacteria in the running state do not change their moving directions as significantly and frequently as those in the tumbling state, we expect that changes in the statistics of δ would report the differences in the run-and-tumble dynamics. The distributions of δ for the different types of micro-pillars are shown in Figure 5A and 5B. Again, we found little difference in the distribution of δ outside the cutoff circle (with ε = 4.8 μm), with all of them showing higher frequencies at low δ values (Figure 5B). In contrast, the distribution of δ inside the cutoff circle changed significantly for the CCAV and SSPK micro-pillars: a higher population of large values (>60°) appeared (Figure 5A). This observation indicated that bacteria at the vicinity of the CCAV and SSPK micro-pillars changed their run-and-tumble dynamics, with a higher tumbling probability.

In addition, we investigated how the average change of moving direction of the bacteria depends on the distance of the bacteria to the surface of the micro-pillars (Δr). As shown in Figure 5C and 5D, we confirmed that δ increased dramatically by ~3-fold as Δr decreased for the SSPK and CCAV micro-pillars, and only moderately for the CVEX micro-pillars. In contrast, the δ–Δr curve remained roughly flat for the CIRC micro-pillars and the control. We also note that these results were robust: varying the cutoff from 3.2 μm (10 pixels) to 6.4 μm (20 pixels) did not change the results significantly (Figure S3).

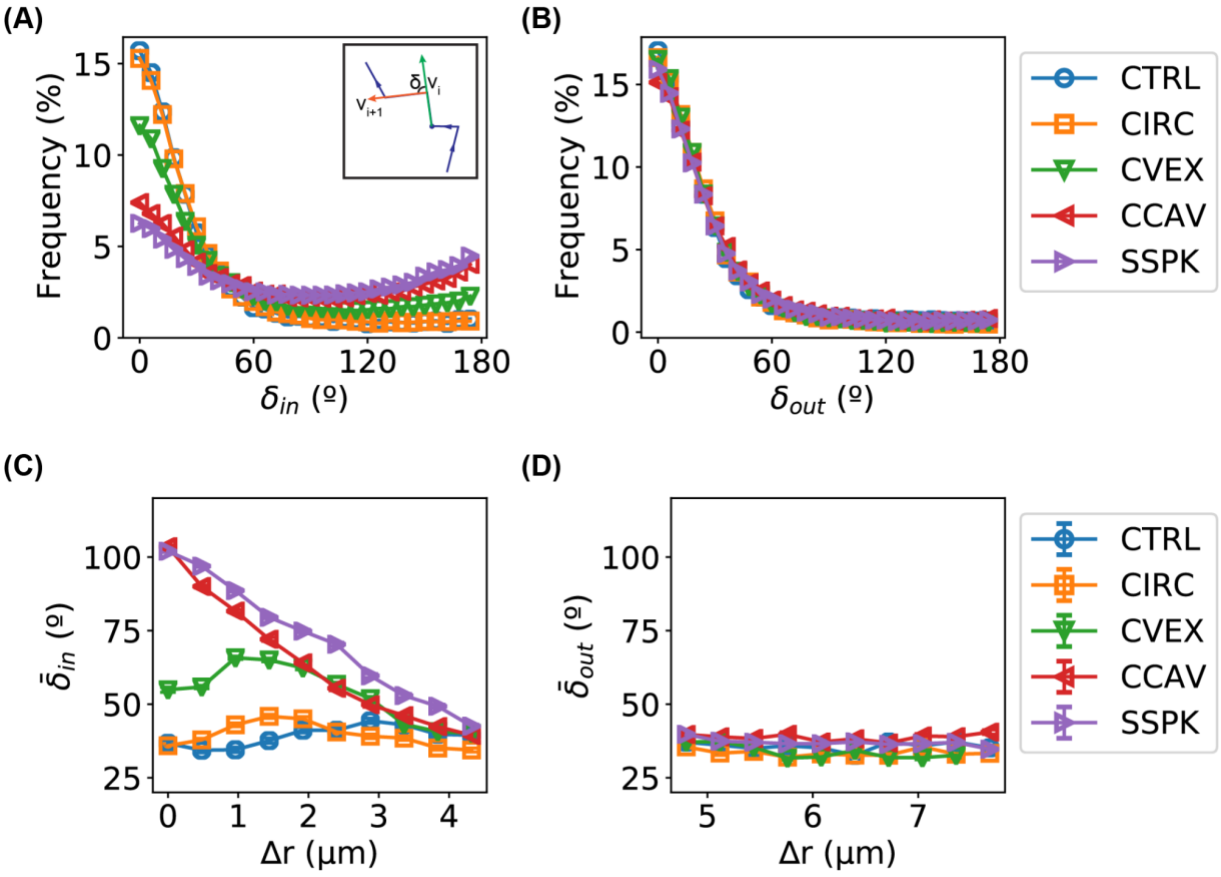

Figure 5. Comparison of the change of moving direction (δ) of bacteria when interacting with micro-pillars with different surface features. (**A, B**) Distribution of directional change of bacteria inside (δ_{in}) or outside (δ_{out}) a virtual cutoff boundary (ε = 4.8 μm). Inset: illustration of the directional change δ. (**C, D**) Dependence of mean directional change of bacteria on the distance of the bacteria to the surface of the micro-pillars. Error bars (smaller than the symbols) represent the standard errors of the means.

Approaching angle of bacteria

Furthermore, we analyzed the approaching angle of bacteria towards the micro-pillars. The approaching angle ϕ is defined as the angle between velocity vector of the bacteria and the tangent of the micro-pillars at the point nearest to the bacteria (inset of Figure 6A). The rationale of this ϕ-based analysis is three-fold: (1) it has been reported that bacteria (and micro-swimmers) were prone to move along smooth pillars / posts, which have been used to guide the motion of

micro-swimmers [25,31]. (2) It was of interest to investigate the scattering between microorganisms and micro-pillars [53–56]. (3) This analysis will provide a direct and independent way to cross-verify the previous observation of the change of run-and-tumble dynamics of the bacteria.

For this analysis, we also included the control (i.e., without any micro-pillars) by considering a virtual smooth micro-pillar with a diameter of 20 μm at the center of the field of view. Because the moving direction of bacteria is expected to be random for the control (assuming the number of bacteria is high enough), we expected that the distribution of the approaching angle is uniform, which was confirmed from our experiments (Figure 6A and 6B, blue circles). In addition, the distributions of ϕ outside the cutoff circle (ε = 4.8 μm) for all the micro-pillars were roughly flat.

At the vicinity of the micro-pillars, the CIRC micro-pillars (with smooth surface) showed significantly higher frequencies at low approaching angles (Figure 6A, orange squares), indicating that the bacteria moved along the surface of the micro-pillars, consistent with previous reports [31]. A similar phenomenon was observed for the CVEX micro-pillars (Figure 6A). However, much shallower distributions of the approaching angle were measured for the CCAV and SSPK micro-pillars, suggesting that the moving directions of the bacteria were more random around the CCAV and SSPK micro-pillars, and implying that the bacteria randomized their directions (i.e., tumbling) when they interacted with the CCAV and SSPK micro-pillars. This is consistent with the conclusions from the δ-based analysis (Figure 5). Furthermore, this result was confirmed by the dependence of the approaching angle on the distance of the bacteria to the surfaces of the micro-pillars (Figure 6C and 6D). Again, different cutoffs gave similar results (Figure S4).

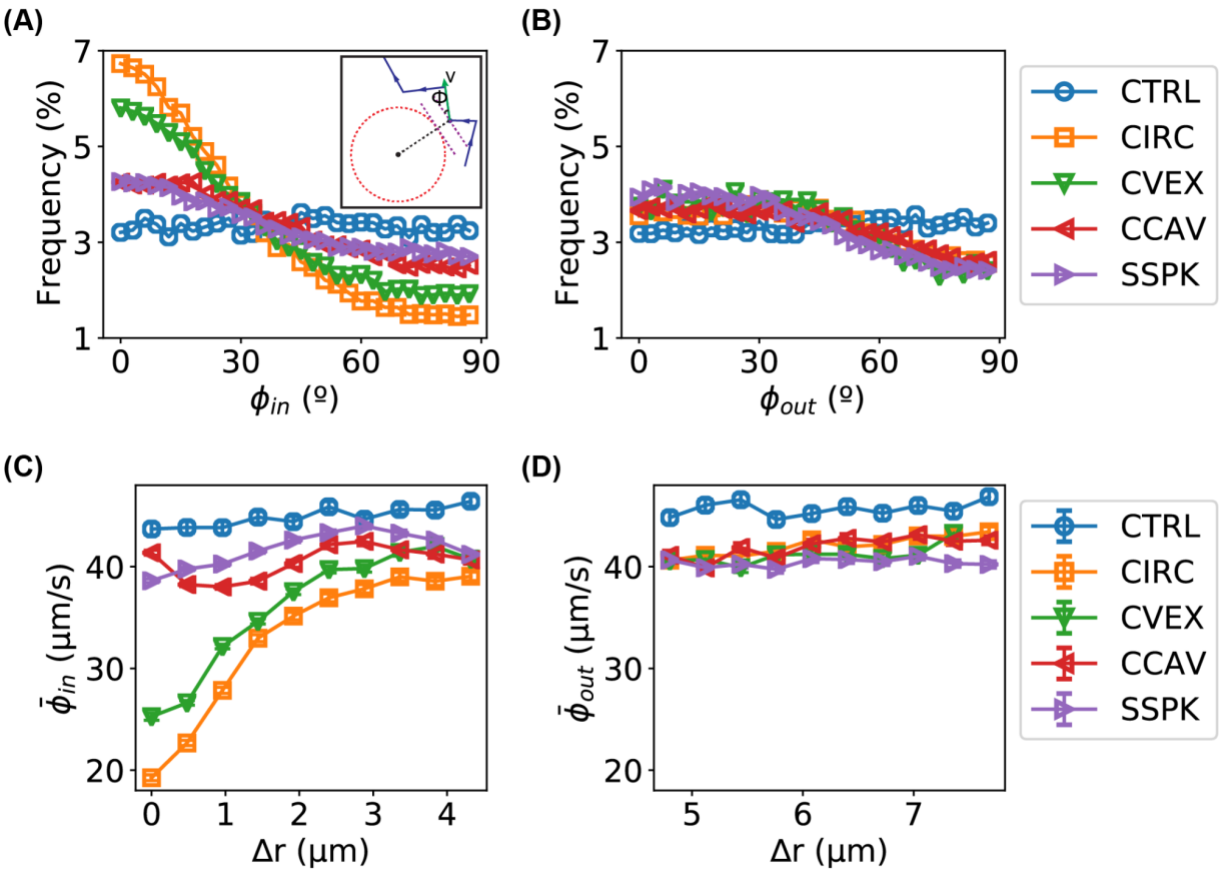

Figure 6. Comparison of the approaching angle (ϕ) of bacteria when interacting with micro-pillars with different surface features. (**A, B**) Distribution of the approaching angle of bacteria inside (ϕ_{in}) or outside (ϕ_{out}) a virtual cutoff boundary (ε = 4.8 µm). Inset: illustration of the approaching angle ϕ. (**C, D**) Dependence of mean approaching angle of bacteria on the distance of the bacteria to the surface of the micro-pillars. Error bars (smaller than the symbols) represent the standard errors of the means.

Numerical simulation of bacterial motion in the presence of micro-pillars

To understand the experimental observations in this study, we ran numerical simulations for the motion of bacteria in the absence and presence of micro-pillars based on an active Brownian motion model developed by Volpe et al. [49]. Briefly, each bacterium was modeled as a micro-sphere with radius R undergoing (1) directional translation with speed *v*, (2) translational Brownian diffusion with a translational diffusion coefficient $D_T = \frac{k_B T}{6\pi\eta R}$, (3) constant rotation with angular velocity Ω, and (4) rational diffusion for orientation of the micro-sphere with a rotational diffusion coefficient $D_R = \frac{k_B T}{8\pi\eta R^3}$. In addition, reflective boundary conditions described by Volpe et al. [49] were used to account for the interactions between bacteria and micro-pillars. As the main difference lies between the CIRC and SSPK micro-pillars, we focused on them in the simulations. In the simulations, the sizes of the bacteria and the micro-pillars (Figure 7A) were similar to those in the experiments.

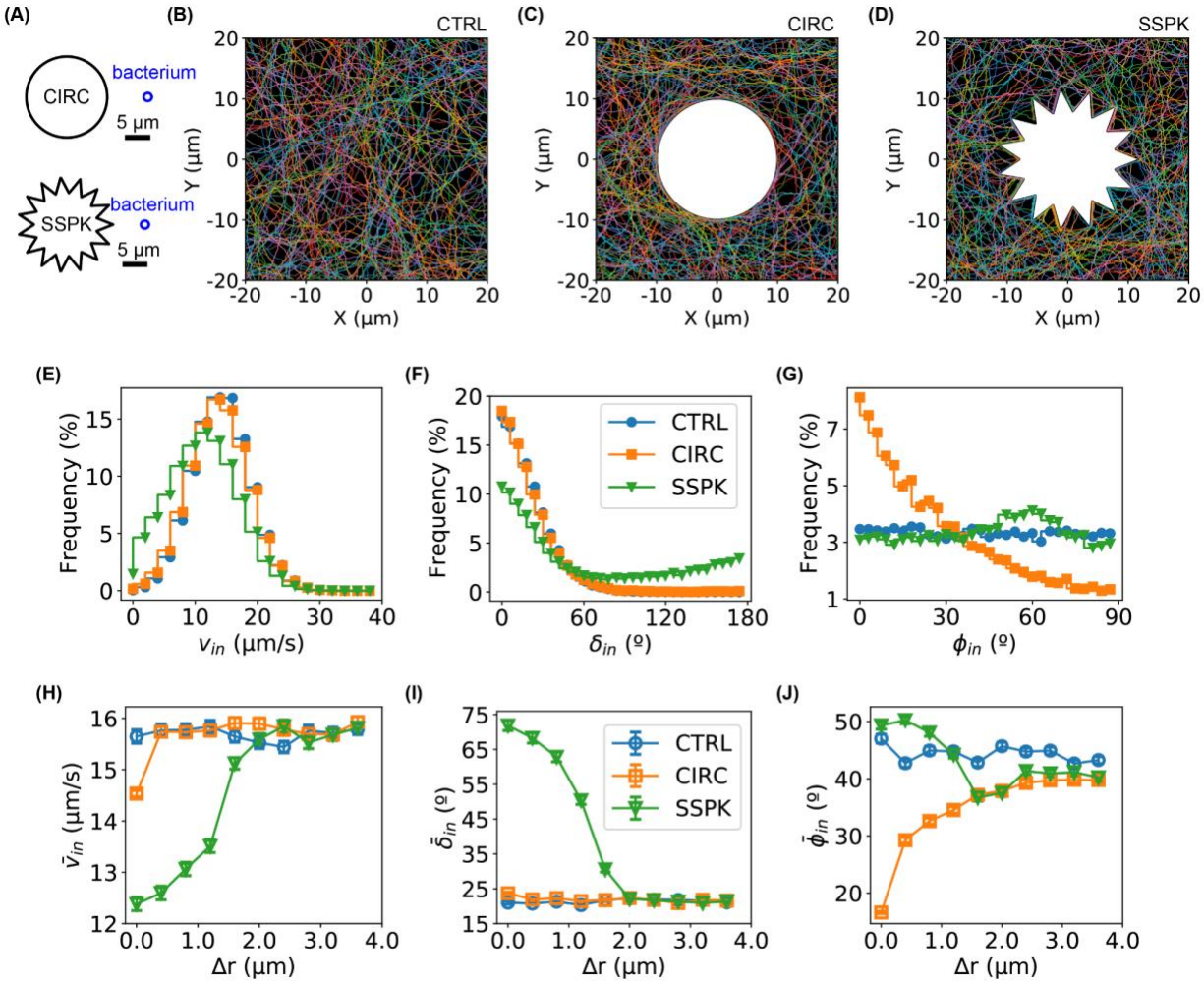

Figure 7. Simulated results for bacteria interacting with micro-pillars with two surface features (CIRC and SSPK). (**A**) Sizes of the bacteria (blue) and micro-pillars (black) in the simulations. (**B–D**) Random examples of simulated trajectories of individual bacteria in the (**B**) absence and (**C, D**) presence of micro-pillars with CIRC or SSPK surface features. Different colors indicate different trajectories. (**E–J**) Comparison of simulated bacteria when interacting with micro-pillars with CIRC or SSPK surface features in terms of (**E, H**) instantaneous velocity – v, (**F, I**) change of moving direction – δ, and (**G, J**) approaching angle – ϕ.

Examples of simulated bacterial trajectories in the absence and presence of CIRC and SSPK micro-pillars are shown in Figure 7B–7D. In these simulations, we took R = 1 μm/s, T = 300 K, η = 10^{-3} Pa·s, and Ω = 0 rad/s. The chosen size of the bacteria in the simulation was in the same order of *E. coli* bacteria [57], although the bacterial shape was spherical instead of rod-shaped. The simulated trajectories appeared similar to the experimental results (Figure 3). More importantly, we found that results from the simulations were consistent with the experiments by quantifying and comparing the bacterial velocity v, the change of moving direction δ, and the approaching angle ϕ. The simulated bacteria showed lower instantaneous velocities (Figure 7E and 7H) and higher changing rate of moving directions (Figure 7F and 7I) at the vicinity of the SSPK micro-pillars, while the CIRC micro-pillars had little effect. In addition, the simulations showed that the approaching angles of bacteria were more random for the SSPK than the CIRC micro-pillars (Figure 7G and 7J). In contrast, the simulations showed similar results for bacteria

outside the cutoff (ε = 4.8 μm) for the control, CIRC and SSPK micro-pillars (Figure S5). These results were consistent with our experimental observations (Figure 4–6), indicating that the model of active micro-swimmers and simple geometric interactions between bacteria and micro-pillars were sufficient for understanding the experimental results. It is worth noting that nonzero angular velocity gave similar results (Figure S6, Ω = 0.1 rad/s).

Conclusions

To summarize, we investigated and quantified how *E. coli* bacteria interact with circular micro-pillars with different geometric modifications. In this study, we focused on four surface features: smooth circles (CIRC), flower-like convex ripples (CVEX), sprocket-like concave ripples (CCAV), and pointed gear-like sharp spikes (SSPK). We examined in detail the motion of bacteria around the micro-pillars and observed significant differences in the bacterial behaviors around the different micro-pillars. We quantified the bacterial behaviors using several parameters, including the bacterial velocity (v), the change of bacterial direction (δ), and the approaching angle (ϕ) of bacteria towards the micro-pillars, and characterized their dependencies on the distance of bacteria to the surface of the micro-pillars. We found that the sharp spikes had the largest effects. Lastly, to understand the experimental observation, we performed numerical simulations based on the active Brownian motion model, in which a particle undergoes translational and rotational diffusions in combination with directional motion and rotation. The simulations showed that the observed differences among the micro-pillars with different surface modifications could be attributed to geometric effects.

In a previous work by Mok et al. [20], it was reported that a concave boundary could reduce the accumulation of bacteria by more than 50% compared to a flat surface. Here we showed that, on the other hand, the concave surface may also trap bacteria, although the trapping effect was less significant than the micro-pillars with sharp spikes. Cell accumulation needs to be avoided in certain applications to prevent the formation of biofilm and biofouling. However, the capability of trapping bacteria and other microbes may be a desired feature in other situations. For example, release-based surface coatings with bactericidal reagents (e.g. antibiotics, silver ions, etc.) may require trapping bacteria for a short time for the reagents to take effect.

We used the model developed by Volpe et al. [49] for running the simulations to understand our experimental results. Although this model treats rod-shaped *E. coli* bacteria as spheres, its successful application in this study indicates that it is not necessary to generalize the model to non-spherical particles in the current scenario. In addition, it implies that the previously reported magic angle formed between the rod-shaped bacteria and surfaces [31] does not play a significant role in the current study, although we cannot exclude its indirect role in the “reflection” mechanism during the collision of the bacteria with the surfaces in the simulations. We expect that Volpe’s model is applicable to other situations. It would be interesting to apply the model to fully understand the behavior of bacteria in mazes or other complex geometries.

A recent theoretical and numerical study investigated the diffusive transport of active particles / micro-swimmers in an obstacle lattice [54]. As the micro-pillars used in this work were arranged as arrays / lattices, it would be interesting to experimentally verify the predictions in the previous report by varying the size and separation of the micro-pillars. In addition, it would be exciting to experimentally examine the transport of bacteria in random arrays of obstacles using the current system, which is expected to facilitate the understanding of how bacteria and microbes navigate through porous media, such as soils and gels.

A single material (OrmoComp) was used for all the four different types of micro-pillars in the current study. This material itself did not significantly affect the bacterial behavior. For example, as shown in Figure 4 and 5, the bacterial velocities and changes of moving directions were similar for bacteria near the CIRC micro-pillars compared to those in the absence of any micro-pillars (i.e., the control). In addition, due to the use of the same material, comparisons of bacterial behaviors at the vicinity of the different types of micro-pillars would exclude the effects from the material itself. On the other hand, we note that, in addition to geometry and shape, bacterial behavior in general depends on the material and other properties (e.g., composition, surface properties and coatings), which are interesting to investigate in the future.

In this study, we made passive, short-term observations on the motion of bacteria in the presence of micro-pillars with different surface features. It would also be exciting to examine how the surface features affect the bacterial behavior around the micro-pillars when active flows are present, as well as how the bacterial behavior depends on the flow rate. In addition, it has been reported that micro-pillars may facilitate the formation of bacterial streamers encased in EPS matrices, the timescale of which spans over several orders. It would be interesting to explore and quantify how different geometric / surface features play a role in the formation of such streamers in both short term and long term. We expect that the system and analysis from the current work will facilitate such studies.

Acknowledgment

This work was supported by the National Science Foundation (grant no. CBET 1826642, IIP 2129225, and OIA-1457888) and the Arkansas Biosciences Institute (grant no. ABI-0189, ABI-0226, ABI-0277, ABI-0326, ABI-2021, ABI-2022, and ABI-SL 3693). We are also grateful for support from the Arkansas High Performance Computing Center (AHPCC), which is funded in part by the National Science Foundation (grant no. 0722625, 0959124, 0963249, and 0918970) and the Arkansas Science and Technology Authority.

References

[1] H.C. Berg, Motile Behavior of Bacteria, Phys. Today. 53 (2000) 24–29. https://doi.org/10.1063/1.882934.

[2] Y. Sowa, R.M. Berry, Bacterial flagellar motor., Q. Rev. Biophys. 41 (2008) 103–132. https://doi.org/10.1017/S0033583508004691.

[3] Z. Zhao, Y. Zhao, X.-Y. Zhuang, W.-C. Lo, M.A.B. Baker, C.-J. Lo, F. Bai, Frequent pauses in Escherichia coli flagella elongation revealed by single cell real-time fluorescence imaging., Nat. Commun. 9 (2018) 1885. https://doi.org/10.1038/s41467-018-04288-4.

[4] N. Wadhwa, H.C. Berg, Bacterial motility: machinery and mechanisms, Nat. Rev. Microbiol. (2021) 1–13. https://doi.org/10.1038/s41579-021-00626-4.

[5] D.B. Kearns, A field guide to bacterial swarming motility, Nat. Rev. Microbiol. 8 (2010) 634–644. https://doi.org/10.1038/nrmicro2405.

[6] R.M. Harshey, Bacterial Motility on a Surface: Many Ways to a Common Goal, Annu. Rev. Microbiol. 57 (2003) 249–273. https://doi.org/10.1146/annurev.micro.57.030502.091014.

[7] P.D. Frymier, R.M. Ford, H.C. Berg, P.T. Cummings, Three-dimensional tracking of motile bacteria near a solid planar surface, Proc. Natl. Acad. Sci. 92 (1995) 6195–6199. https://doi.org/10.1073/pnas.92.13.6195.
[8] C.N. Dominick, X.-L. Wu, Rotating Bacteria on Solid Surfaces without Tethering., Biophys. J. 115 (2018) 588–594. https://doi.org/10.1016/j.bpj.2018.06.020.
[9] J.C. Conrad, Physics of bacterial near-surface motility using flagella and type IV pili: implications for biofilm formation, Res. Microbiol. 163 (2012) 619–629. https://doi.org/10.1016/j.resmic.2012.10.016.
[10] N.A. Licata, B. Mohari, C. Fuqua, S. Setayeshgar, Diffusion of bacterial cells in porous media., Biophys. J. 110 (2016) 247–257. https://doi.org/10.1016/j.bpj.2015.09.035.
[11] T. Bhattacharjee, S.S. Datta, Bacterial hopping and trapping in porous media, Nat. Commun. 10 (2019) 2075. https://doi.org/10.1038/s41467-019-10115-1.
[12] U.U. Ghosh, H. Ali, R. Ghosh, A. Kumar, Bacterial streamers as colloidal systems: Five grand challenges, J. Colloid Interface Sci. 594 (2021) 265–278. https://doi.org/10.1016/j.jcis.2021.02.102.
[13] I. Biswas, M. Sadrzadeh, A. Kumar, Impact of bacterial streamers on biofouling of microfluidic filtration systems, Biomicrofluidics. 12 (2018) 044116. https://doi.org/10.1063/1.5025359.
[14] E. Rossi, M. Paroni, P. Landini, Biofilm and motility in response to environmental and host-related signals in Gram negative opportunistic pathogens, J. Appl. Microbiol. 125 (2018) 1587–1602. https://doi.org/10.1111/jam.14089.
[15] S.B. Guttenplan, D.B. Kearns, Regulation of flagellar motility during biofilm formation, FEMS Microbiol. Rev. 37 (2013) 849–871. https://doi.org/10.1111/1574-6976.12018.
[16] M. Molaei, M. Barry, R. Stocker, J. Sheng, Failed Escape: Solid Surfaces Prevent Tumbling of Escherichia coli, Phys. Rev. Lett. 113 (2014) 068103. https://doi.org/10.1103/PhysRevLett.113.068103.
[17] A.P. Berke, L. Turner, H.C. Berg, E. Lauga, Hydrodynamic Attraction of Swimming Microorganisms by Surfaces, Phys. Rev. Lett. 101 (2008) 038102. https://doi.org/10.1103/PhysRevLett.101.038102.
[18] G. Li, J.X. Tang, Accumulation of Microswimmers near a Surface Mediated by Collision and Rotational Brownian Motion, Phys. Rev. Lett. 103 (2009) 078101. https://doi.org/10.1103/PhysRevLett.103.078101.
[19] G. Li, J. Bensson, L. Nisimova, D. Munger, P. Mahautmr, J.X. Tang, M.R. Maxey, Y.V. Brun, Accumulation of swimming bacteria near a solid surface, Phys. Rev. E. 84 (2011) 041932. https://doi.org/10.1103/PhysRevE.84.041932.
[20] R. Mok, J. Dunkel, V. Kantsler, Geometric control of bacterial surface accumulation, Phys. Rev. E. 99 (2019) 052607. https://doi.org/10.1103/PhysRevE.99.052607.
[21] P. Galajda, J. Keymer, P. Chaikin, R. Austin, A Wall of Funnels Concentrates Swimming Bacteria, J. Bacteriol. 189 (2007) 8704–8707. https://doi.org/10.1128/JB.01033-07.
[22] A. Sokolov, M.M. Apodaca, B.A. Grzybowski, I.S. Aranson, Swimming bacteria power microscopic gears, Proc. Natl. Acad. Sci. 107 (2010) 969–974. https://doi.org/10.1073/pnas.0913015107.
[23] R.D. Leonardo, L. Angelani, D. Dell'Arciprete, G. Ruocco, V. Iebba, S. Schippa, M.P. Conte, F. Mecarini, F.D. Angelis, E.D. Fabrizio, Bacterial ratchet motors, Proc. Natl. Acad. Sci. 107 (2010) 9541–9545. https://doi.org/10.1073/pnas.0910426107.
[24] G. Lambert, D. Liao, R.H. Austin, Collective Escape of Chemotactic Swimmers through Microscopic Ratchets, Phys. Rev. Lett. 104 (2010) 168102. https://doi.org/10.1103/PhysRevLett.104.168102.
[25] M.S. Davies Wykes, X. Zhong, J. Tong, T. Adachi, Y. Liu, L. Ristroph, M.D. Ward, M.J. Shelley, J. Zhang, Guiding microscale swimmers using teardrop-shaped posts., Soft Matter. 13 (2017) 4681–4688. https://doi.org/10.1039/c7sm00203c.

[26] J. Fabrega, R. Zhang, J.C. Renshaw, W.-T. Liu, J.R. Lead, Impact of silver nanoparticles on natural marine biofilm bacteria., Chemosphere. 85 (2011) 961–966. https://doi.org/10.1016/j.chemosphere.2011.06.066.
[27] J.-L. Yang, Y.-F. Li, X. Liang, X.-P. Guo, D.-W. Ding, D. Zhang, S. Zhou, W.-Y. Bao, N. Bellou, S. Dobretsov, Silver nanoparticles impact biofilm communities and mussel settlement., Sci. Rep. 6 (2016) 37406. https://doi.org/10.1038/srep37406.
[28] M.A. Radzig, V.A. Nadtochenko, O.A. Koksharova, J. Kiwi, V.A. Lipasova, I.A. Khmel, Antibacterial effects of silver nanoparticles on gram-negative bacteria: influence on the growth and biofilms formation, mechanisms of action., Colloids Surf. B Biointerfaces. 102 (2013) 300–306. https://doi.org/10.1016/j.colsurfb.2012.07.039.
[29] K. Markowska, A.M. Grudniak, K.I. Wolska, Silver nanoparticles as an alternative strategy against bacterial biofilms., Acta Biochim. Pol. 60 (2013) 523–530.
[30] K. Beppu, Z. Izri, J. Gohya, K. Eto, M. Ichikawa, Y.T. Maeda, Geometry-driven collective ordering of bacterial vortices., Soft Matter. 13 (2017) 5038–5043. https://doi.org/10.1039/c7sm00999b.
[31] O. Sipos, K. Nagy, R. Di Leonardo, P. Galajda, Hydrodynamic trapping of swimming bacteria by convex walls., Phys. Rev. Lett. 114 (2015) 258104. https://doi.org/10.1103/PhysRevLett.114.258104.
[32] A. Valiei, A. Kumar, P.P. Mukherjee, Y. Liu, T. Thundat, A web of streamers: biofilm formation in a porous microfluidic device, Lab. Chip. 12 (2012) 5133–5137. https://doi.org/10.1039/C2LC40815E.
[33] M. Hassanpourfard, Z. Nikakhtari, R. Ghosh, S. Das, T. Thundat, Y. Liu, A. Kumar, Bacterial floc mediated rapid streamer formation in creeping flows, Sci. Rep. 5 (2015) 13070. https://doi.org/10.1038/srep13070.
[34] V.R. Krishnamurthi, J. Chen, Y. Wang, Silver ions cause oscillation of bacterial length of Escherichia coli., Sci. Rep. 9 (2019) 11745. https://doi.org/10.1038/s41598-019-48113-4.
[35] A.A. Sadoon, Y. Wang, Anomalous, non-Gaussian, viscoelastic, and age-dependent dynamics of histonelike nucleoid-structuring proteins in liveEscherichia coli, Phys. Rev. E. 98 (2018) 042411. https://doi.org/10.1103/PhysRevE.98.042411.
[36] M. Alqahtany, P. Khadka, I. Niyonshuti, V.R. Krishnamurthi, A.A. Sadoon, S.D. Challapalli, J. Chen, Y. Wang, Nanoscale reorganizations of histone-like nucleoid structuring proteins in Escherichia coli are caused by silver nanoparticles, Nanotechnology. 30 (2019) 385101. https://doi.org/10.1088/1361-6528/ab2a9f.
[37] Photonic Professional GT2: World's highest resolution 3D printer, (n.d.). https://www.nanoscribe.com/en/products/photonic-professional-gt2 (accessed July 20, 2021).
[38] M. Afshar-Mohajer, M. Zou, Multi-Scale In Situ Tribological Studies of Surfaces with 3D Textures Fabricated via Two-Photon Lithography and Replica Molding, Adv. Mater. Interfaces. 7 (2020) 2000299. https://doi.org/10.1002/admi.202000299.
[39] A.D. Edelstein, M.A. Tsuchida, N. Amodaj, H. Pinkard, R.D. Vale, N. Stuurman, Advanced methods of microscope control using μManager software., J. Biol. Methods. 1 (2014). https://doi.org/10.14440/jbm.2014.36.
[40] A. Edelstein, N. Amodaj, K. Hoover, R. Vale, N. Stuurman, Computer control of microscopes using μManager., Curr. Protoc. Mol. Biol. Chapter 14 (2010) Unit14.20. https://doi.org/10.1002/0471142727.mb1420s92.
[41] J. Schindelin, I. Arganda-Carreras, E. Frise, V. Kaynig, M. Longair, T. Pietzsch, S. Preibisch, C. Rueden, S. Saalfeld, B. Schmid, J.-Y. Tinevez, D.J. White, V. Hartenstein, K. Eliceiri, P. Tomancak, A. Cardona, Fiji: an open-source platform for biological-image analysis., Nat. Methods. 9 (2012) 676–682. https://doi.org/10.1038/nmeth.2019.
[42] C.A. Schneider, W.S. Rasband, K.W. Eliceiri, NIH Image to ImageJ: 25 years of image analysis., Nat. Methods. 9 (2012) 671–675. https://doi.org/10.1038/nmeth.2089.

[43] A. Rogers, I.I. Niyonshuti, A. Cai, F. Wang, M. Benamara, J. Chen, Y. Wang, Real-Time Imaging of Laser-Induced Nanowelding of Silver Nanoparticles in Solution, J. Phys. Chem. C. 125 (2021) 10422–10430. https://doi.org/10.1021/acs.jpcc.1c00184.
[44] S. van der Walt, J.L. Schönberger, J. Nunez-Iglesias, F. Boulogne, J.D. Warner, N. Yager, E. Gouillart, T. Yu, scikit-image contributors, scikit-image: image processing in Python., PeerJ. 2 (2014) e453. https://doi.org/10.7717/peerj.453.
[45] Sternberg, Biomedical Image Processing, Computer. 16 (1983) 22–34. https://doi.org/10.1109/MC.1983.1654163.
[46] N. Kanopoulos, N. Vasanthavada, R.L. Baker, Design of an image edge detection filter using the Sobel operator, IEEE J. Solid-State Circuits. 23 (1988) 358–367. https://doi.org/10.1109/4.996.
[47] E. Nosal, Flood-fill algorithms used for passive acoustic detection and tracking, in: 2008 New Trends Environ. Monit. Using Passive Syst., 2008: pp. 1–5. https://doi.org/10.1109/PASSIVE.2008.4786975.
[48] D.B. Allan, T. Caswell, N.C. Keim, C.M. van der Wel, Trackpy: Trackpy V0.4.1, Zenodo. (2018). https://doi.org/10.5281/zenodo.1226458.
[49] G. Volpe, S. Gigan, G. Volpe, Simulation of the active Brownian motion of a microswimmer, Am. J. Phys. 82 (2014) 659–664. https://doi.org/10.1119/1.4870398.
[50] U. Alon, L. Camarena, M.G. Surette, B. Aguera y Arcas, Y. Liu, S. Leibler, J.B. Stock, Response regulator output in bacterial chemotaxis., EMBO J. 17 (1998) 4238–4248. https://doi.org/10.1093/emboj/17.15.4238.
[51] A.E. Pottash, R. McKay, C.R. Virgile, H. Ueda, W.E. Bentley, TumbleScore: Run and tumble analysis for low frame-rate motility videos., Biotechniques. 62 (2017) 31–36. https://doi.org/10.2144/000114493.
[52] C.D. Amsler, Use of computer-assisted motion analysis for quantitative measurements of swimming behavior in peritrichously flagellated bacteria., Anal. Biochem. 235 (1996) 20–25. https://doi.org/10.1006/abio.1996.0086.
[53] M. Contino, E. Lushi, I. Tuval, V. Kantsler, M. Polin, Microalgae scatter off solid surfaces by hydrodynamic and contact forces., Phys. Rev. Lett. 115 (2015) 258102. https://doi.org/10.1103/PhysRevLett.115.258102.
[54] T. Jakuszeit, O.A. Croze, S. Bell, Diffusion of active particles in a complex environment: Role of surface scattering., Phys. Rev. E. 99 (2019) 012610. https://doi.org/10.1103/PhysRevE.99.012610.
[55] V. Kantsler, J. Dunkel, M. Polin, R.E. Goldstein, Ciliary contact interactions dominate surface scattering of swimming eukaryotes, Proc. Natl. Acad. Sci. 110 (2013) 1187–1192. https://doi.org/10.1073/pnas.1210548110.
[56] A. Morin, D. Lopes Cardozo, V. Chikkadi, D. Bartolo, Diffusion, subdiffusion, and localization of active colloids in random post lattices, Phys. Rev. E. 96 (2017) 042611. https://doi.org/10.1103/PhysRevE.96.042611.
[57] U. Moran, R. Phillips, R. Milo, SnapShot: key numbers in biology., Cell. 141 (2010) 1262-1262.e1. https://doi.org/10.1016/j.cell.2010.06.019.